DIRECT NOISE PREDICTION AND CONTROL OF AN INSTALLED LARGE LOW-SPEED RADIAL FAN

M. Sanjosé[1]*, S. Moreau[1]

[1]Université de Sherbrooke, Département de Génie Mécanique
2500 boulevard de l'Université, Sherbrooke, J1K2R1, QC, Canada
marlene.sanjose@usherbrooke.ca

Introduction

Low-speed radial fan are used in many residential applications for ventilation, cooling and heating systems. The noise level produced by these systems is one of the main concerns for customers. Thus, aeroacoustic predictions are required by the manufacturers at the conception level. Aero-acoustic sources are multiple in complex systems. Broadband noise component is produced by a wide range of turbulent excitations while tonal noise component is rather related to large coherent flow structures strongly depending on the installation. In the present work, unsteady compressible numerical simulations are used to predict tonal and broadband noise components of the acoustic spectra for a radial low-speed fan installed in a complex module typical of many ventilation systems in transportation applications. Very few numerical tools allow to capture at affordable computational cost, both the tonal and broadband sources and the far-field propagation as it requires to capture large structures related to the installation to very small turbulent structures that appear in boundary layers, and a wide range of wave-numbers on a large computational domain [1, 2]. Even fewer involve the complete installation system around the fan. The present methodology relies on direct noise generation and propagation using the Lattice-Boltzmann Method on the complete installation and the fast turnaround of the simulations allow testing several passive or semi-active control strategies.

Methodology

The investigated large radial fan is installed in a large module as presented in Fig. 1(a). The latter involves a large plenum with several entries and a stack of heat exchangers connected at the outlet to two rectangular ducts with varying sections. The rotational speed is 1200 rpm yielding a low maximum Mach number of 0.05. The whole module is then placed in a large anechoic room with a hard solid ground as in the experiment. The plenum is related to the system circular duct through an elliptic adapter. The configuration has been tested in the semi-anechoic room at Université de Sherbrooke as shown in Fig. 1(b), where volume flow-rates in the two outlet ducts were measured simultaneously with sound pressure levels in the far-field. The flow rates have been estimated following the ISO-3966 standard, e.g. the velocity has been measured along several lines at the outlet ducts with a Pitot tube. The far-field acoustic pressure has been measured at several locations around the mock-up, but the present study will mostly focus at two positions M1 and M2 above the outlets sections as shown in Fig. 1(c).

The actual flow recirculation in the actual hemi-anechoic room is therefore properly mimicked. The computational domain is meshed using cubic voxels only, with several voxel refinement (VR) zones, some of them are highlighted in pink and yellow in Fig. 1(a). Several mesh resolutions especially near the rotor have been investigated leading to a final mesh of 88 million voxels. The Exa Powerflow 4.4 solver is used to perform the compressible Very Large Eddy Simulation (VLES) of this configuration. The interface between the rotor part and the stationary part of the domain is a sliding mesh interface as explained in [2].

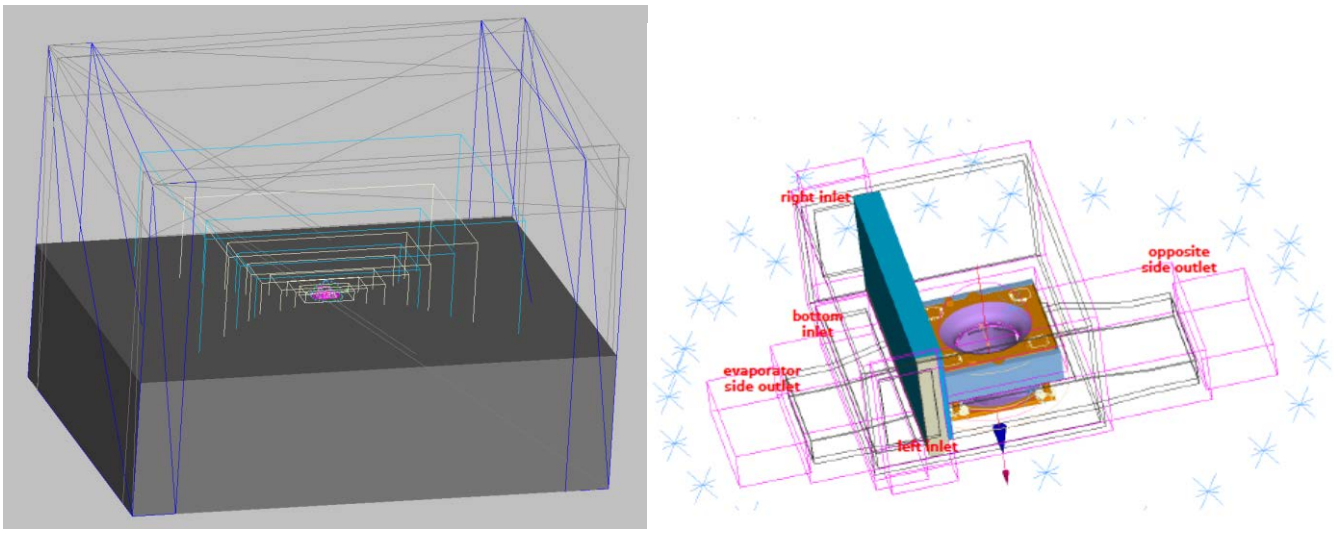

a) Numerical investigated configuration and set-up.

(b) Measured experimental configuration in the UdS semi-anechoic room.

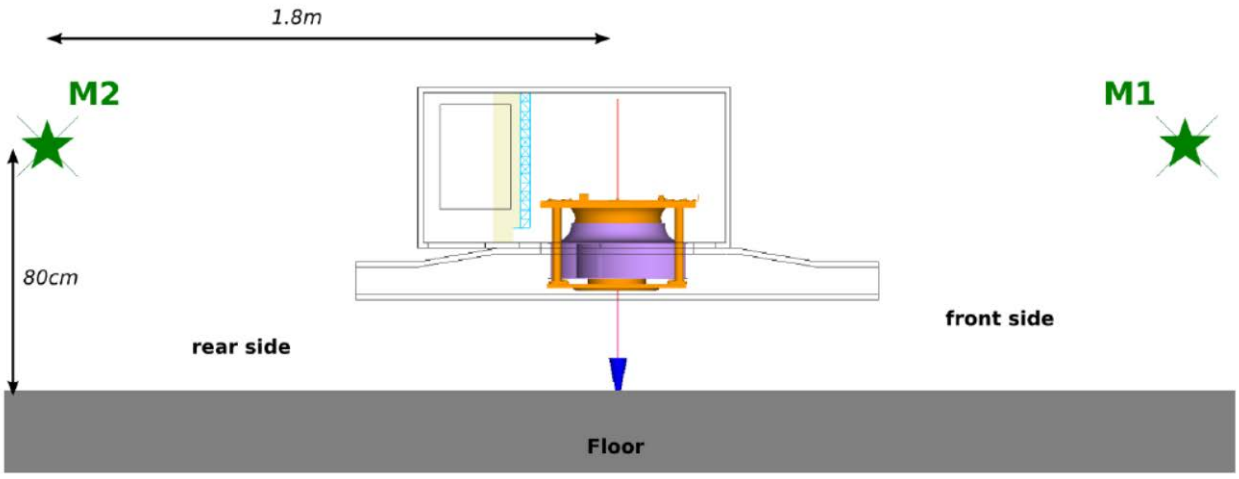

(c) Reference microphone positions.

Figure 1: Installed low-speed radial fan investigated in the present study.

The time step is selected by the solver to ensure a CFL number based on the speed of sound of one in the smallest voxels. This leads to a time-step of 1.65 10^{-6} s. The torque and the flow-rate are monitored during the simulation to evaluate the convergence of the system towards a steady state. Steady flow-rates on the inlets and outlets of the fan system were obtained after 2 fan revolutions. In addition to the two microphone probes M1 and M2 the static pressure at different probe locations (blue crosses in Fig. 1(a)) around the mockup are recorded to extract sound directivity. Unsteady pressures were recorded for at least 0.8 s to obtain a well resolved spectrum down to 100 Hz.

In addition to the baseline case, several passive noise control devices have also been tested. First a geometrical modification of the hub has been suggested based on the airflow analysis below. The latter has also suggested a better flow-conditioning at the fan inlet, which led to the addition of a filter on top of the fan system. The porosity of this filter has been experimentally determined. Finally an obstruction has been added below the filter to provide tonal noise control [3, 4]. All the numerically tested configurations are summarized in Table 1.

Calculation Name	Geometry details	Rotating Speed
Baseline	Initial setup	1200 rpm
New-Hub	Modified hub	1200 rpm
Filter	Initial setup with filter	1200 rpm
Filt-Obstr	Initial setup with filter and flow obstruction	1200 rpm

Table 1: Installed low-speed radial fan investigated in the present study.

Preliminary results

The global performances of the installed fan are compared with the experimental measurements in Table 2. The flow distribution between the two sides is well represented but the numerical model underpredicts the experimental estimate by 12%. Fig. 2 shows that this discrepancy is mostly caused by the boundary layer resolution on the upper and lower wall of the ducts. They are numerically overestimated because of a lack of local grid resolution. Yet as the velocity distributions in the duct core are well predicted no further grid refinement was achieved.

	Experiments	Numerical Simulation	Difference (%)
Evaporator side	$0.50\,m^3/s$	$0.44\,m^3/s$	12
Opposite side	$0.48\,m^3/s$	$0.42\,m^3/s$	12.5

Table 2: Installed low-speed radial fan investigated in the present study.

The overall flow structure within the module is shown in Fig. 3. The particular geometry of the inlet chamber generates large distortions ingested by the fan. The incoming flows coming from the three fold inlets generate turbulent structures caused by their mixing that can be identified by the Λ_2 criterion in Fig. 3(a). The flow goes through the evaporator modeled by a porous medium that yields a uniform velocity profile along the whole width of the inlet box. This side entrance even if homogeneous generates a strong distorted flow pattern at the inlet of the fan as can be seen in Figs 3(a) and 3(b). The fluid closest to the fan goes directly into the convergent while the more remote lines have to go all around the inlet box to finally enter the fan. These variations in flow paths generate strong distortions upstream of the fan. Such distortions are typical source of tonal noise. A first control device to be introduced is therefore to limit this strong distortion and straighten the flow at the inlet with a filter.

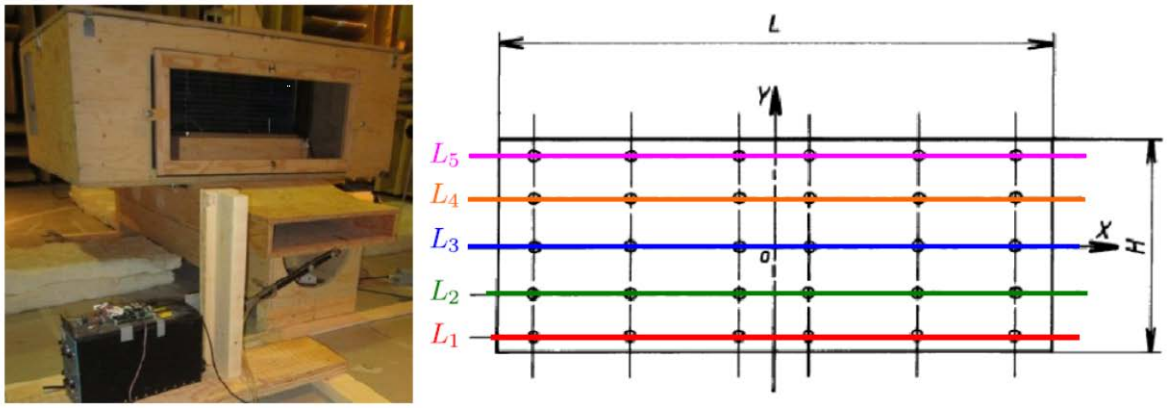

a) Experimental measurements of the velocity distribution over the outlet sections.

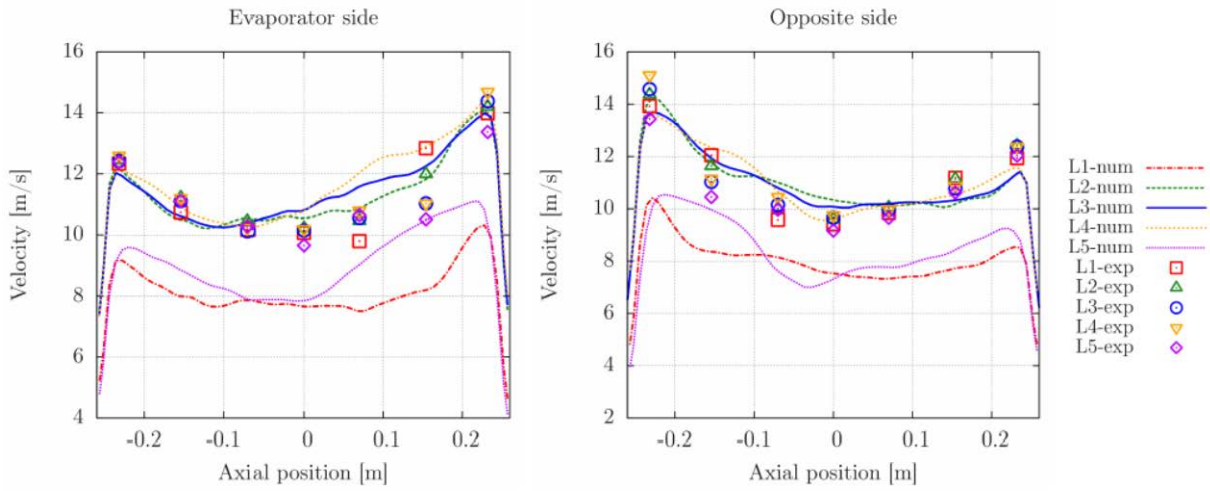

(b) Velocity distribution at the mock-up outlets from the Baseline simulations.

Figure 2: Global performance comparisons.

Looking closer to the fan, a flow detachment also appears close to the motor and hub. This flow detachment is strongly unstable during the fan rotation and the position of the stagnation point on the top part of the motor varies slightly over time. These two observations have triggered a second control device: a more streamlined hub shape.

Preliminary acoustic results on the baseline configuration are shown for the two microphones M1 and M2. The acoustic spectra computed from the static pressure history recorded by the probes shown in Fig. 1(c) are compared with acoustic measurements in Fig. 4. The numerical spectra agree very well with the experimental spectra up to 3000 Hz. The comb of tones between 3000 Hz and 5000 Hz that appears in the experiments is related to the power supply converter from 50 to 60 Hz. Above 5000 Hz the numerical errors limit the decay at high frequencies. The very good agreement of the spectrum shape at low frequency proves that the installation effects of the mock-up are well reproduced in the numerical setup.

The next step will to compare these baseline results with the suggested modifications from the above flow analysis.

References

[1] T. Carolus, M. Schneider, and H. Reese, 2007, "Axial flow fan broad-band noise and prediction", *J. Sound Vib.*, 300 (1-2):50–70.

[2] F. Perot, M.-S. Kim, S. Moreau, & M. Henner, 2010, "Direct aeroacoustics prediction of a low speed axial fan", in *16th AIAA/CEAS Aeroacoust. Conf.*, 3887, Stockholm, Sweden.

[3] F. Perot, M.S. Kim, V. Le Goff, V. Carniel, Y. Goth & C. Chassaignon, 2012, “Numerical Optimization of the Tonal Noise of a Backward Centrifugal Fan Using a Flow Obstruction”, *Fan 2012*, ,Senlis, France.
[4] S. Magne, M. Sanjose, S. Moreau, A. Berry, “Aeroacoustic Simulation of the Acoustic Modulation to Control Tonal Noise with Flow Obstruction,” 20th AIAA/CEAS Aeroacoustics Conference, Atlanta, USA, June 2014.

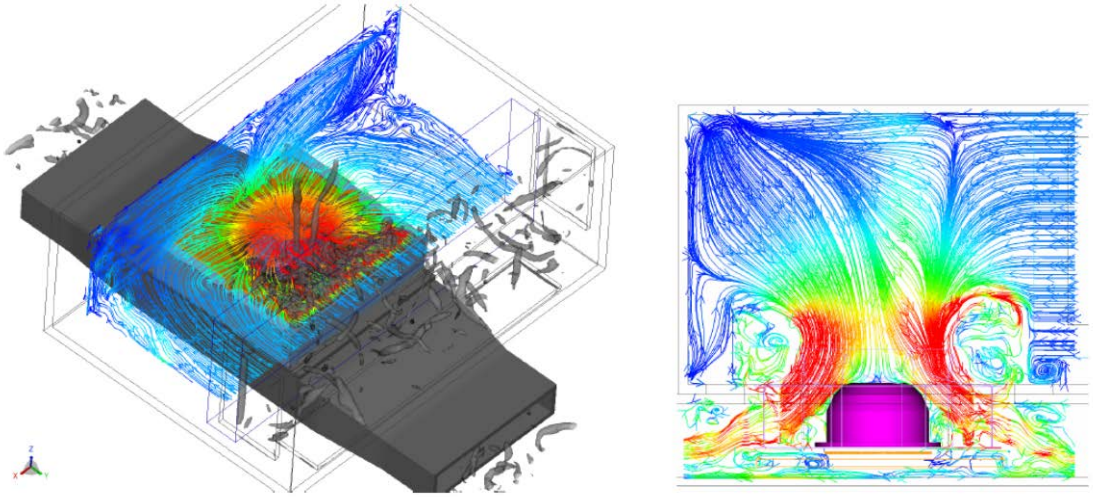

(a) Global view of the mock-up. (b) Close view in the fan bowl

Figure 3: Module flow structure.

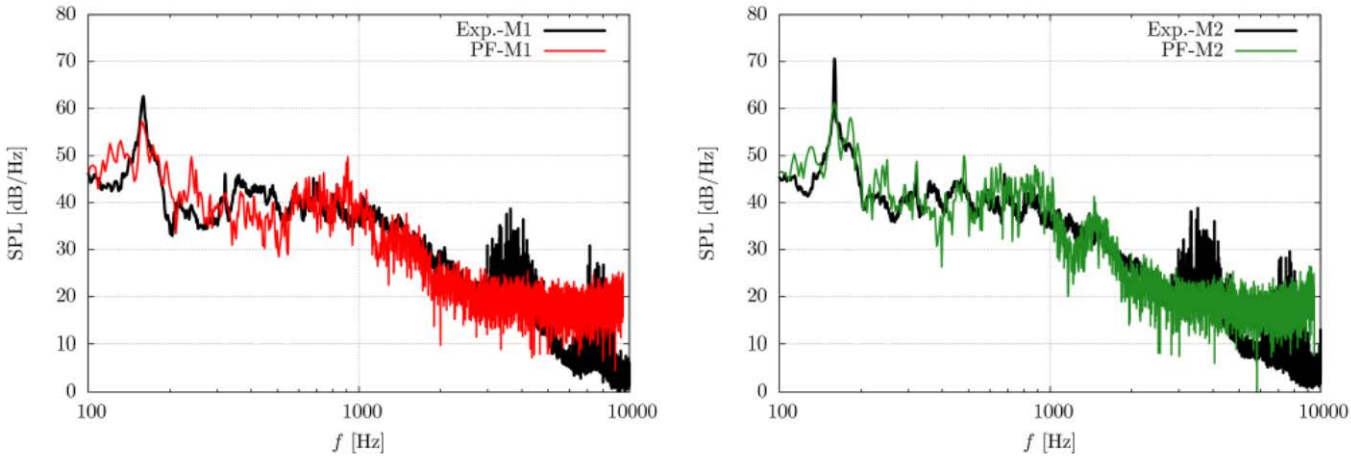

Figure 4: Acoustic comparisons on microphones M1 and M2.